

Disco Intelligent Omni-Surfaces: 360° Fully-Passive Jamming Attacks

Huan Huang, *Member, IEEE*, Hongliang Zhang, *Member, IEEE*, Jide Yuan, *Member, IEEE*, Luyao Sun, Yitian Wang, Weidong Mei, *Member, IEEE*, Boya Di, *Member, IEEE*, Yi Cai, *Senior Member, IEEE*, and Zhu Han *Fellow, IEEE*

Abstract—Intelligent omni-surfaces (IOSs) with 360° electromagnetic radiation significantly improves the performance of wireless systems, while an adversarial IOS also poses a significant potential risk for physical layer security. In this paper, we propose a “DISCO” IOS (DIOS) based fully-passive jammer (FPJ) that can launch omnidirectional fully-passive jamming attacks. In the proposed DIOS-based FPJ, the interrelated refractive and reflective (R&R) coefficients of the adversarial IOS are randomly generated, acting like a “DISCO ball” that distributes wireless energy radiated by the base station. By introducing active channel aging (ACA) during channel coherence time, the DIOS-based FPJ can perform omnidirectional fully-passive jamming without neither jamming power nor channel knowledge of legitimate users (LUs). To characterize the impact of the DIOS-based FPJ, we derive the statistical characteristics of DIOS-jammed channels based on two widely-used IOS models, i.e., the constant-amplitude model and the variable-amplitude model. Consequently, the asymptotic analysis of the ergodic achievable sum rates under the DIOS-based omnidirectional fully-passive jamming is given based on the derived stochastic characteristics for both the two IOS models. Based on the derived analysis, the omnidirectional jamming impact of the proposed DIOS-based FPJ implemented by a constant-amplitude IOS does not depend on either the quantization number or the stochastic distribution of the DIOS coefficients, while the conclusion does not hold on when a variable-amplitude IOS is used. Numerical results based on one-bit quantization of the IOS phase shifts are provided to verify the effectiveness of the derived theoretical analysis. The proposed DIOS-based FPJ can not only launch omnidirectional fully-passive jamming, but also improve the jamming impact by about 55% at 10 dBm transmit power per LU.

Index Terms—Channel aging, jamming attacks, intelligent omni-surface, multi-user MISO (MU-MISO), physical layer security.

I. INTRODUCTION

Due to the inherent broadcast and superposition properties of wireless channels, wireless systems are vulnerable to ma-

licious physical-layer attacks such as physical-layer jamming, which is a type of denial-of-service (DoS) attacks [2]–[4]. In wireless systems, physical-layer jamming can be easily launched by an active jammer (AJ), which inflicts intentional jamming/interference attacks to block the wireless communication between the access point (AP) and the legitimate users (LUs). Typical AJs can be divided into the following categories: 1) constant AJs, 2) intermittent AJs [5], 3) reactive AJs [6], and 4) adaptive AJs [7]. These AJs have the inherent energy limitation because the AJs require to broadcast intentional jamming/interference, such as pseudorandom noise or modulated Gaussian waveforms, over an open wireless channel. Therefore, an important metric of AJs is the development of strategies to maximize the duration and area of effective jamming while minimizing jamming power. However, the AJs inevitably consume a certain amount of jamming energy to prevent LUs from communicating with legitimate APs.

Recently, reconfigurable intelligent surfaces (RISs) have attracted increasing attention as a promising candidate technology for the future sixth generation (6G) wireless communications [8]–[10]. Existing works mainly focus on the use of RISs to improve system performance, e.g. minimizing energy efficiency [11], [12] or maximizing spectrum efficiency [13], [14], where the RIS coefficients should be carefully designed according to the channel state information (CSI). Unlike legitimate RISs, adversarial RISs, the illegitimate utilization of RISs [15] poses a significant detrimental impact on wireless systems, which needs to be given increasing attention.

A. Related Works

Some existing works have focused on the detrimental impact of adversarial RISs. For example, the work [17] has reported an adversarial RIS-based passive jammer (PJ) that destructively adds the reflected path signal to the direct path signal to minimize the received power, i.e., to minimize the signal-to-noise ratio (SNR). Then the communications between the legitimate AP and its LU in the single-user multiple-input single-output (SU-MISO) system are blocked. Moreover, the authors in [18] investigated the use of an adversarial RIS to jam an multi-user multiple-input single-output (MU-MISO) system. Similarly, the attacker must carefully calculate the reflective coefficients of the adversarial RIS in order to minimize the sum rate, i.e., to minimize the signal-to-interference-plus-noise ratio (SINR). Although these adversarial RIS can jam LUs without consuming jamming power, CSI of all wireless

A portion of this work was published in [1].

H. Huang, J. Yuan, L. Sun, Y. Wang, and Y. Cai are with the School of Electronic and Information Engineering, Soochow University, Suzhou, Jiangsu 215006, China (e-mail: hhuang1799@gmail.com, jide_yuan@suda.edu.cn, lysun02@163.com, ytwang41@stu.suda.edu.cn, yicai@ieee.org).

H. Zhang and B. Di are with the School of Electronics, Peking University, Beijing 100871, China (email: hongliang.zhang92@gmail.com, diboya@pku.edu.cn).

W. Mei is with the National Key Laboratory of Wireless Communications, University of Electronic Science and Technology of China, Chengdu 611731, China (e-mail: wmei@uestc.edu.cn).

Z. Han is with the Department of Electrical and Computer Engineering, University of Houston, Houston, TX 77004 USA, and also with the Department of Computer Science and Engineering, Kyung Hee University, Seoul, South Korea, 446-701. (email: hanzhu22@gmail.com).

TABLE I
COMPARISON OF DIFFERENT JAMMERS

Reference	Mechanism	Jamming power	Channel knowledge	Jamming area
[17], [18]	Optimize RIS coefficients to minimize SNR or SINR	Not Required	Required	Reflective side
[19]–[21], [23]–[26]	Break channel reciprocity in TDD systems	Not Required	Not Required	Reflective side

channels, including the wireless channels between legitimate APs and LUs, must be known at the adversarial RIS. Due to the passive nature of RISs, it is unrealistic to assume that the illegitimate RIS knows the CSI, especially the CSI of the wireless channels between legitimate APs and LUs.

To address the limitation of adversarial RISs in acquiring the CSI, fully-passive jammers (FPJs) have been proposed [19]–[21], which can launch jamming attacks without relying on either jamming power or CSI. The concept of FPJ was first proposed in [19], where an adversarial RIS with random and time-varying reflective coefficients acts like a “DISCO ball” and is therefore called a DISCO RIS (DRIS) [20]. The use of DRIS causes active channel aging (ACA) and then fully-passive jamming is generated [21]. Note that the ACA is different from traditional channel aging (CA) [22] that occurs due to time variations in RF propagation and computational delays between the moment the wireless channels are acquired at the AP and when they are applied for precoding. Moreover, some works investigated the introduction of DIRSs to break key consistency in channel reciprocity-based key generation [23]–[25] or to break channel reciprocity-based communications [26] in time division duplex (TDD) wireless systems. For more clarity, we list and compare these adversarial RIS-based jamming schemes in Table I.

It can be seen from Table I, although the DRIS-based FPJs can launch fully-passive jamming attacks without relying on either jamming power or LU channel knowledge, they can only jam the LUs located on the reflective side of the DRIS. Namely, there are blind jamming areas, where the LUs located on the refractive side of the DRIS are completely unable to be jammed by the DRIS-based FPJ. Immediately following the studies on RISs, intelligent omni-surfaces (IOSs) are being introduced into wireless communications to achieve 360° performance improvement by enabling the simultaneous reflection and refraction [27]–[33]. It should be noted that an IOS is not the same as two independent reflective RISs back to back [27], [32], [33], because there is an additional constraint between the refractive and reflective (R&R) coefficients of each IOS element. Due to this additional constraint, an IOS can not be directly introduced into the DRIS-based FPJ [19]–[21] to implement omnidirectional fully-passive jamming. Considering this constraint of an IOS, the work [1] first proposed the concept of omnidirectional FPJ, which introduces a DISCO IOS (DIOS) to implement 360° fully-passive jamming attacks. However, the authors in [1] only demonstrated the impact of the DIOS-based FPJ on an MU-MISO system through simulations, without providing a theoretical analysis.

B. Contributions and Organization

In this work, we propose a DIOS-based FPJ that can launch 360° fully-passive jamming attacks without relying on either jamming power or LUs’ channel knowledge. To quantify the impact of these omnidirectional fully-passive jamming attacks, the quantitative analysis is performed. The main contributions are summarized as follows:

- We investigate the downlink rate of an MU-MISO system jammed by the proposed DIOS-based FPJ. In the proposed DIOS-based FPJ, the DIOS remains “silent” during each pilot transmission (PT) phase, where the term “silent” refers to the wireless signals being perfectly absorbed by the adversarial DIOS [34]. Then, the DIOS randomly changes its R&R coefficients during the subsequent data transmission (DT) phase. In other words, the DIOS with random and time-varying R&R coefficients acts like a “DISCO ball” that distributes the AP transmit power in random directions. As a result, the AP-LU channels change rapidly, causing serious inter-user interference, referred to as active channel age (ACA).
- Two widely-used IOS models, i.e., the constant-amplitude IOS model and the variable-amplitude IOS model, are introduced into the investigation of the DIOS-based FPJ. In the two IOS models, the R&R phase shifts of the IOS elements are discrete and interrelated. In the constant-amplitude IOS model, we assume that the R&R amplitudes of each IOS element are constant and equal. Yet, in the variable-amplitude IOS model, the R&R amplitudes of each IOS element are assumed to be dependent and different for different R&R phase shifts, and the R&R amplitudes of each IOS element are also not equal, alternating due to the energy conservation constraint. For both constant-amplitude and variable-amplitude IOS models, we perform the proposed DIOS-based FPJ under the constraint that the R&R coefficients are related.
- To quantify the impact of the omnidirectional fully-passive jamming, we give the asymptotic analysis of the achievable sum rates under the above two IOS assumptions, i.e., the constant-amplitude DIOS assumption and the variable-amplitude DIOS assumption. First, the statistical characteristics of the DIOS-jammed channels are given for both the two DIOS models. Then, the lower bounds of the downlink rates are derived for both the refractive-side LUs and the reflective-side LUs based on the derived statistical characteristics.
- Based on the detailed asymptotic analysis, we present some unique properties of the proposed DIOS-based FPJ. For instance, the jamming impact is not dependent on either the quantization bits or the distribution of the

R&R phase shifts when the constant-amplitude DIOS is exploited. However, when the variable-amplitude DIOS is used, the jamming impact depends on the quantization bits and the distribution. Since the jamming impacts on the refractive-side LUs and the reflective-side LUs are related by energy conservation, we can carefully design a distribution to balance the impacts of the DIOS-based omnidirectional fully-passive jamming attacks on the refractive-side LUs and the reflective-side LUs.

The rest of this paper is organized as follows. In Section II, the downlink of an MU-MISO system jammed by the proposed DIOS-based FPJ is first modeled, where the performance metric used to quantify the omnidirectional jamming impact is given. Then, all wireless channels involved are modeled. In Section III, the statistical characteristics of the time-varying R&R DIOS-jammed channels are derived based on two widely-used IOS models, i.e., the constant-amplitude model and the variable-amplitude model. Then, the asymptotic analysis of the proposed DIOS-based FPJ is performed, where the lower bounds of ergodic achievable R&R sum rates are derived. Simulation results are presented in Section IV to demonstrate the effectiveness of the derived asymptotic analysis and the jamming impact of the proposed DIOS-based FPJ. Finally, the main conclusions are summarized in Section V.

Notation: We employ bold capital letters for a matrix, e.g., \mathbf{W}_{ZF} , lowercase bold letters for a vector, e.g., $\mathbf{w}_{ZF,k}$, and italic letters for a scalar, e.g., K . The superscripts $(\cdot)^T$ and $(\cdot)^H$ represent the transpose and the Hermitian transpose, respectively, and the symbols $\|\cdot\|$ and $|\cdot|$ represent the Frobenius norm and the absolute value, respectively.

II. SYSTEM DESCRIPTION

In this section, we first describe an MU-MISO system under the jamming attacks launched by the DIOS-based FPJ. Then, all wireless channels involved are built.

A. Disco IOS Based Fully-Passive jammer

Fig. 1 schematically shows an MU-MISO system attacked by the proposed DIOS-based FPJ, where the DIOS-based FPJ launches omnidirectional fully-passive jamming attacks without relying on jamming power and CSI. We assume that the legitimate AP equipped with an N_A -element uniform linear array (ULA) communicates with total K LUs denoted by $\mathcal{K} = \{1, \dots, K\}$. Furthermore, we assume that K_t LUs termed as $\mathcal{K}_t = \{1, \dots, K_t\}$ and K_r LUs termed as $\mathcal{K}_r = \{1, \dots, K_r\}$ are respectively located on the refractive and reflective (R&R) side of the DIOS, where $K = K_r + K_t$. Similar to the deployment in [1], [19]–[21], the DIOS is implemented close to the AP.

Generally, during the channel coherence time in an MU-MISO system, the AP designs the transmit beamforming used in the *DT* phase based on the CSI acquiring from the *PT* phase. Furthermore, we assume that the length of a *DT* phase is C times longer than that of a *PT* phase, i.e., $T_D = CT_P$. Similar to the setting in [20], [21], the DIOS is turned off during the *PT* phase and then turned on during the *DT* phase with random and time-varying R&R coefficients, where the period during

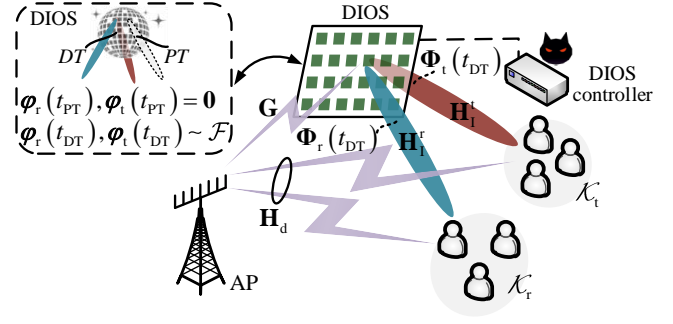


Fig. 1. An illustration of an MU-MISO system jammed by DISCO intelligent omni-surface (DIOS) based fully-passive jamming attacks, where the DIOS is turned off during the *pilot transmission (PT)* and then turned on during *data transmission (DT)* phases.

which the R&R coefficients are changing is about the same as the length of the *PT* phase T_P . Mathematically, we denote R&R passive beamforming as $\Phi_t(t) = \text{diag}(\varphi_t(t))$ and $\Phi_r(t) = \text{diag}(\varphi_r(t))$ [16], [27], [28], where the random and time-varying R&R vectors are respectively expressed as

$$\varphi_t(t) = [\alpha_1^t(t) e^{j\varphi_1^t(t)}, \dots, \alpha_{N_D}^t(t) e^{j\varphi_{N_D}^t(t)}], \quad (1)$$

and

$$\varphi_r(t) = [\alpha_1^r(t) e^{j\varphi_1^r(t)}, \dots, \alpha_{N_D}^r(t) e^{j\varphi_{N_D}^r(t)}]. \quad (2)$$

In (1) and (2), the R&R amplitudes $\alpha_m^t(t)$ and $\alpha_m^r(t)$ of the m -th DIOS element ($m = 1, \dots, N_D$) are a function of their corresponding R&R phase shifts $\varphi_m^t(t)$ and $\varphi_m^r(t)$ [27], [33]. Furthermore, $\alpha_m^t(t)$ and $\alpha_m^r(t)$ satisfy the energy conservation constraint, i.e., $|\alpha_m^t(t)|^2 + |\alpha_m^r(t)|^2 = 1$ [28].

In practice, an IOS is an ultra-thin surface composed of multiple sub-wavelength elements whose R&R coefficients are controlled by simple programmable PIN or varactor diodes [8]. We assume that the programmable PINs are used to implement the DIOS, whose ON/OFF behavior only allows for the creation of discrete phase shifts. Therefore, we denote the b -bit refractive phase set as $\Theta_t = \{\theta_1^t, \dots, \theta_{2^b}^t\}$ and the b -bit reflective phase set as $\Theta_r = \{\theta_1^r, \dots, \theta_{2^b}^r\}$, respectively. Note that an IOS has an additional constraint compared to a RIS that the R&R phase shifts $\varphi_m^t(t)$ and $\varphi_m^r(t)$ are inter-related [32], [33]. Namely, $\varphi_m^t(t)$ is $\theta_m^t \in \Theta_t$ if $\varphi_m^r(t)$ takes $\theta_m^r \in \Theta_r$. Moreover, the R&R amplitudes are assume to take from the sets $\Lambda_t = \{\xi_1^t, \dots, \xi_{2^b}^t\}$ and $\Lambda_r = \{\xi_1^r, \dots, \xi_{2^b}^r\}$, where $|\xi_s^r|^2 + |\xi_s^t|^2 = 1, s = 1, \dots, 2^b$.

Transmit Beamforming Design: In the *PT* phase of each channel coherence time, the CSI estimated by using methods such as the least squares (LS) algorithm [35] is expressed as $\mathbf{H}_{PT}^H = \mathbf{H}_d^H = [\mathbf{h}_{d,1}, \dots, \mathbf{h}_{d,K}]^H \in \mathbb{C}^{K \times N_A}$, i.e., the overall direct channel between the K LUs and the AP. Based on the CSI of \mathbf{H}_{PT} , the AP then designs the transmit beamforming used to send signals to the LUs during the following *DT* phase. Without loss of generality, we assume that the AP uses zero-forcing (ZF) beamforming to transmit LUs' signals during the

following DT phase. Mathematically, the ZF beamforming can be given by [36], [37]

$$\mathbf{W}_{\text{ZF}} = \frac{\mathbf{H}_d(\mathbf{H}_d^H \mathbf{H}_d)^{-1} \mathbf{P}^{\frac{1}{2}}}{\left\| \mathbf{H}_d(\mathbf{H}_d^H \mathbf{H}_d)^{-1} \right\|} = [\mathbf{w}_{\text{ZF},1}, \dots, \mathbf{w}_{\text{ZF},K}], \quad (3)$$

where $\mathbf{P} = \text{diag}(p_1, \dots, p_K)$ represents the power allocation matrix, and $\|\mathbf{P}\|^2 \leq P_0$. It is worth noting that the optimal power allocation matrix can be computed by using the water-filling algorithm [37]. For convenience, we further assume that $p_1 = \dots = p_K = P_0$

Active Channel Aging: When \mathbf{W}_{ZF} has been calculated according to (3), it is used by the AP in the consequent DT phase to transmit signals to the LUs. In traditional MU-MISO systems, wireless channels can be assumed to remain unchanged during the channel coherence time. However, in the MU-MISO system under the omnidirectional DISCO jamming attacks, the DIOS R&R coefficients are randomly changed whose period is about T_P and much smaller than that the length of channel coherence time T_C . As a result, ACA is introduced, and then the channel reciprocity of the wireless channels in traditional TDD systems is broken. Mathematically, the time-varying channel during the DT phase can be written as

$$\mathbf{H}_{\text{DT}} = \mathbf{H}_d + \begin{bmatrix} \mathbf{H}_{\text{D}}^t(t_{\text{DT}}) \\ \mathbf{H}_{\text{D}}^r(t_{\text{DT}}) \end{bmatrix} = \mathbf{H}_d + \begin{bmatrix} \mathbf{G}^H \Phi_t(t_{\text{DT}}) \mathbf{H}_{\text{I}}^t \\ \mathbf{G}^H \Phi_r(t_{\text{DT}}) \mathbf{H}_{\text{I}}^r \end{bmatrix}, \quad (4)$$

where $(\mathbf{H}_{\text{D}}^t(t_{\text{DT}}))^H = [\mathbf{h}_{\text{D},1}^t(t_{\text{DT}}), \dots, \mathbf{h}_{\text{D},K_t}^t(t_{\text{DT}})]^H \in \mathbb{C}^{K_t \times N_A}$ and $(\mathbf{H}_{\text{D}}^r(t_{\text{DT}}))^H = [\mathbf{h}_{\text{D},1}^r(t_{\text{DT}}), \dots, \mathbf{h}_{\text{D},K_r}^r(t_{\text{DT}})]^H \in \mathbb{C}^{K_r \times N_A}$ stand for the overall R&R DIOS-jammed channels in the DT phase, respectively. In (4), $\mathbf{G} \in \mathbb{C}^{N_D \times N_A}$ is the channel between the AP and the DIOS, and $\mathbf{H}_{\text{I}}^t = [\mathbf{h}_{\text{I},1}^t, \dots, \mathbf{h}_{\text{I},K_t}^t] \in \mathbb{C}^{N_D \times K_t}$ and $\mathbf{H}_{\text{I}}^r = [\mathbf{h}_{\text{I},1}^r, \dots, \mathbf{h}_{\text{I},K_r}^r] \in \mathbb{C}^{N_D \times K_r}$ are the R&R channels between the DIOS and the LUs.

Based on (4), one can see that the channel reciprocity assumption no longer holds. More specifically, we define the ACA channel \mathbf{H}_{ACA} as

$$\mathbf{H}_{\text{ACA}} = \mathbf{H}_{\text{DT}} - \mathbf{H}_{\text{PT}} = \begin{bmatrix} \mathbf{H}_{\text{D}}^t(t_{\text{DT}}) \\ \mathbf{H}_{\text{D}}^r(t_{\text{DT}}) \end{bmatrix}. \quad (5)$$

Ergodic Achievable Downlink Rate: According to (4), the signals received at the k_t -th refractive-side LU and the k_r -th reflective-side LU in the DT phase ($T_P < t_{\text{DT}} \leq T_C$) are expressed as [1], [27]

$$y_{\text{DT},k_t}^t = (\mathbf{h}_{\text{d},k_t}^H + \mathbf{h}_{\text{D},k_t}^H) \sum_{u \in \mathcal{K}} \mathbf{w}_{\text{ZF},u} x_{\text{DT},u} + n_{k_t}, \quad (6)$$

and

$$y_{\text{DT},k_r}^r = (\mathbf{h}_{\text{d},k_r}^H + \mathbf{h}_{\text{D},k_r}^H) \sum_{u \in \mathcal{K}} \mathbf{w}_{\text{ZF},u} x_{\text{DT},u} + n_{k_r}, \quad (7)$$

where we assume that the transmit signals for all R&R LUs satisfy $\mathbb{E}[x_{\text{DT},u}^2] = 1, u \in \mathcal{K}$, and $n_{k_t}, n_{k_r} \sim \mathcal{CN}(0, \delta^2)$ are the received AWGN.

According to (6) and (7), the ergodic achievable downlink rate at the k_t -th refractive-side and the k_r -th reflective-side LUs are given by

$$R_{k_t}^t = \log_2(1 + \gamma_{k_t}^t), \quad (8)$$

and

$$R_{k_r}^r = \log_2(1 + \gamma_{k_r}^r). \quad (9)$$

More specifically, the SINRs of the k_t -th refractive-side and the k_r -th reflective-side LUs are expressed as [38]

$$\gamma_{k_t}^t = \frac{\mathbb{E} \left[\left| (\mathbf{h}_{\text{d},k_t} + \mathbf{h}_{\text{D},k_t}^t(t_{\text{DT}}))^H \mathbf{w}_{\text{ZF},k_t} \right|^2 \right]}{\mathbb{E} \left[\sum_{u \neq k_t} \left| (\mathbf{h}_{\text{d},k_t} + \mathbf{h}_{\text{D},k_t}^t(t_{\text{DT}}))^H \mathbf{w}_{\text{ZF},u} \right|^2 \right] + \delta^2}, \quad (10)$$

and

$$\gamma_{k_r}^r = \frac{\mathbb{E} \left[\left| (\mathbf{h}_{\text{d},k_r} + \mathbf{h}_{\text{D},k_r}^r(t_{\text{DT}}))^H \mathbf{w}_{\text{ZF},k_r} \right|^2 \right]}{\mathbb{E} \left[\sum_{u \neq k_r} \left| (\mathbf{h}_{\text{d},k_r} + \mathbf{h}_{\text{D},k_r}^r(t_{\text{DT}}))^H \mathbf{w}_{\text{ZF},u} \right|^2 \right] + \delta^2}. \quad (11)$$

where the R&R DIOS-jammed channels can be further given by $(\mathbf{h}_{\text{D},k_t}^t(t_{\text{DT}}))^H = (\mathbf{h}_{\text{I},k_t}^t)^H \Phi_t(t_{\text{DT}}) \mathbf{G}^H$ and $(\mathbf{h}_{\text{D},k_r}^r(t_{\text{DT}}))^H = (\mathbf{h}_{\text{I},k_r}^r)^H \Phi_r(t_{\text{DT}}) \mathbf{G}^H$, respectively.

From (8) and (9), one can see that the DIOS-based FPJ launches omnidirectional fully-passive jamming attacks by randomly generating the time-varying R&R passive beamforming $\Phi_t(t_{\text{DT}})$ and $\Phi_r(t_{\text{DT}})$ to rapidly age wireless channels. The fully-passive jamming is also referred to as active channel aging interference (ACAI) [21]. Consequently, the ergodic achievable sum rate is given by $R_{\text{sum}} = R_{\text{sum}}^t + R_{\text{sum}}^r = \sum_{k_t \in \mathcal{K}_t} R_{k_t}^t + \sum_{k_r \in \mathcal{K}_r} R_{k_r}^r$.

B. Channel Model

In the MU-MISO system attacked by the DIOS-based FPJ, the AP-DIOS channel \mathbf{G} in (4) is constructed based on the near-field model because the DIOS is implemented near to the AP. Mathematically, \mathbf{G} in (4) is modeled as [14], [39]

$$\mathbf{G} = \sqrt{\mathcal{L}_{\mathcal{G}}} \left(\sqrt{\frac{\varepsilon_{\mathcal{G}}}{1 + \varepsilon_{\mathcal{G}}}} \widehat{\mathbf{G}}^{\text{LOS}} + \sqrt{\frac{1}{1 + \varepsilon_{\mathcal{G}}}} \widehat{\mathbf{G}}^{\text{NLOS}} \right), \quad (12)$$

where $\mathcal{L}_{\mathcal{G}}$ is the large-scale channel fading of \mathbf{G} and $\varepsilon_{\mathcal{G}}$ represents the Rician factor for \mathbf{G} . In (12), $\widehat{\mathbf{G}}^{\text{NLOS}}$ follows Rayleigh fading [14], [40], i.e., the elements $[\widehat{\mathbf{G}}^{\text{NLOS}}]_{n,s} \sim \mathcal{CN}(0, 1), n = 1, \dots, N_A, s = 1, \dots, N_D$. Furthermore, the elements of $\widehat{\mathbf{G}}^{\text{LOS}}$ are given by [21], [39]

$$[\widehat{\mathbf{G}}^{\text{LOS}}]_{n,s} = e^{-j \frac{2\pi}{\lambda} (d_{n,s} - d_n)}, \quad (13)$$

where λ is the wavelength of transmit signals, and $d_{n,s}$ and d_n are the distance between the n -th ULA antenna and the s -th DIOS element and the distance between the n -th ULA antenna and the origin of the DIOS, respectively.

Moreover, the R&R DIOS-LU channels \mathbf{H}_{I}^t and \mathbf{H}_{I}^r , and the direct AP-LU channel \mathbf{H}_d (4) are modeled based on the far-field model [40]:

$$\mathbf{H}_{\text{I}}^t = \left[\sqrt{\mathcal{L}_{\text{I},1}^t} \widehat{\mathbf{h}}_{\text{I},1}^t, \dots, \sqrt{\mathcal{L}_{\text{I},K_t}^t} \widehat{\mathbf{h}}_{\text{I},K_t}^t \right], \quad (14)$$

$$\mathbf{H}_{\text{I}}^r = \left[\sqrt{\mathcal{L}_{\text{I},1}^r} \widehat{\mathbf{h}}_{\text{I},1}^r, \dots, \sqrt{\mathcal{L}_{\text{I},K_r}^r} \widehat{\mathbf{h}}_{\text{I},K_r}^r \right], \quad (15)$$

$$\mathbf{H}_d = \left[\sqrt{\mathcal{L}_{\text{d},1}} \widehat{\mathbf{h}}_{\text{d},1}, \dots, \sqrt{\mathcal{L}_{\text{d},K}} \widehat{\mathbf{h}}_{\text{d},K} \right], \quad (16)$$

where $\mathcal{L}_{I,k_t}^t, k_t \in \mathcal{K}_t$, $\mathcal{L}_{I,k_r}^r, k_r \in \mathcal{K}_r$, and $\mathcal{L}_{d,k}, k \in \mathcal{K}$ denote the large-scale channel fading coefficients. The n -th elements in $\widehat{\mathbf{h}}_{I,k_t}^t, \widehat{\mathbf{h}}_{I,k_r}^r$, and $\widehat{\mathbf{h}}_{d,k}$ are modeled as independent and identically distributed (i.i.d.) Gaussian random variables with mean zero and variance 1, and are assumed to be independent over $n, n = 1, \dots, N_A$ [41].

III. ERGODIC ACHIEVABLE DOWNLINK RATE UNDER DIOS-BASED FULLY-PASSIVE JAMMING ATTACKS

In this section, we derive the statistical characteristics of the DIOS-jammed channel to characterize the jamming impact of the DIOS-based FPJ for two IOS models, i.e., the constant-amplitude model and the variable-amplitude model in Section III-A. In Section III-B, we further derive a lower bound of the ergodic achievable downlink rate based on the statistical characteristics of the DIOS-jammed channel.

A. Statistical Characteristics of Active Channel Aging

According to (8) and (9), the time-varying DIOS R&R coefficients fail channel reciprocity. As a result, the ACAI is introduced to launch omnidirectional fully-passive jamming attacks. Therefore, the impact of the DIOS-based FPJ is directly dependent on the characteristics of the time-varying R&R DIOS-jammed channels $\mathbf{H}_D^t(t)$ and $\mathbf{H}_D^r(t)$. We first assume that the DIOS R&R coefficients are constant, i.e., $\alpha_s^t(t) = \alpha_s^r(t) = \frac{\sqrt{2}}{2}, \forall s$. Then, the statistical characteristics of $\mathbf{H}_D^t(t)$ and $\mathbf{H}_D^r(t)$ are given in Proposition 1.

Proposition 1: For a constant-amplitude DIOS, the i.i.d. elements in $\mathbf{H}_D^t(t)$ and $\mathbf{H}_D^r(t)$ converge in distribution to $\mathcal{CN}(0, \mathcal{L}_G \mathcal{L}_{I,k_t}^t N_D / 2)$ and $\mathcal{CN}(0, \mathcal{L}_G \mathcal{L}_{I,k_r}^r N_D / 2)$ as $N_D \rightarrow \infty$, i.e.,

$$[\mathbf{H}_D^t(t)]_{n,k_t} \stackrel{d}{\rightarrow} \mathcal{CN}\left(0, \frac{\mathcal{L}_G \mathcal{L}_{I,k_t}^t N_D}{2}\right), \quad (17)$$

and

$$[\mathbf{H}_D^r(t)]_{n,k_r} \stackrel{d}{\rightarrow} \mathcal{CN}\left(0, \frac{\mathcal{L}_G \mathcal{L}_{I,k_r}^r N_D}{2}\right), \quad (18)$$

where $0 \leq t \leq T_C, n = 1, \dots, N_A, k_t \in \mathcal{K}_t$, and $k_r \in \mathcal{K}_r$.

Proof: See Appendix A. ■

It should be noted that, in practice, the DIOS must have a large number of elements to handle the multiplicative large-scale channel fading in the DIOS-jammed R&R channels. From Proposition 1, a property of the DIOS-based FPJ implemented by a constant-amplitude IOS is that its jamming impact does not depend on nor the number of its phase quantization bits nor the stochastic distribution of the DIOS R&R phase shifts. Namely, we can use a one-bit quantization IOS whose R&R phase shifts follow the simple uniform distribution to effectively implement the DIOS-based PFJ.

For the variable-amplitude IOS model built in Section II-A, we denote the probability of the R&R phase shift φ_s^t and φ_s^r taking the m -th value in Θ , i.e., θ_m as $P_m, \forall s$. As a result, the statistical characteristics in Proposition 1 shift to Proposition 2.

Proposition 2: For a variable-amplitude DIOS, the i.i.d. elements in $\mathbf{H}_D^t(t)$ and $\mathbf{H}_D^r(t)$ converge in distribution to

$\mathcal{CN}(0, \mathcal{L}_G \mathcal{L}_{I,k_t}^t N_D \mu)$ and $\mathcal{CN}(0, \mathcal{L}_G \mathcal{L}_{I,k_r}^r N_D (1 - \mu))$ as $N_D \rightarrow \infty$, i.e.,

$$[\mathbf{H}_D^t(t)]_{n,k_t} \stackrel{d}{\rightarrow} \mathcal{CN}(0, \mathcal{L}_G \mathcal{L}_{I,k_t}^t N_D \mu), \quad (19)$$

and

$$[\mathbf{H}_D^r(t)]_{n,k_r} \stackrel{d}{\rightarrow} \mathcal{CN}(0, \mathcal{L}_G \mathcal{L}_{I,k_r}^r N_D (1 - \mu)), \quad (20)$$

where $\mu = \sum_{m=1}^{2^b} P_m (\xi_m^t)^2 = 1 - \left(\sum_{m=1}^{2^b} P_m (\xi_m^r)^2\right)$.

Proof: See Appendix B. ■

Based on Proposition 2, we can see that the jamming impact of the DIOS-based FPJ implemented by an IOS with variable amplitudes depends on the number of DIOS phase quantization bits and the stochastic distribution of the DIOS R&R phase shifts. Furthermore, the impact on the refractive-side LUs and that on the reflective-side LUs are mutually exclusive, and the trade-off between them can be tuned by stochastic distribution of the DIOS R&R phase shifts.

B. Lower Bound of Ergodic Achievable Downlink Rate

In this section, we aim to quantify the impact of the DIOS-based FPJ on LUs. The ergodic achievable R&R sum rate R_{sum}^t and R_{sum}^r of the refractive-side users and the reflective-side users have been given based on the definitions in (8) and (9). According to (10) and (11), R_{sum}^t and R_{sum}^r can be expressed as

$$\begin{aligned} R_{\text{sum}}^t &= \sum_{k_t \in \mathcal{K}_t} R_{k_t}^t = \sum_{k_t \in \mathcal{K}_t} \log_2(1 + \gamma_{k_t}^t) \\ &= \sum_{k_t \in \mathcal{K}_t} \log_2 \left(1 + \frac{\mathbb{E} \left[\left| (\mathbf{h}_{d,k_t} + \mathbf{h}_{D,k_t}^t(t_{DT}))^H \mathbf{w}_{ZF,k_t} \right|^2 \right]}{\mathbb{E} \left[\sum_{u \neq k_t} \left| (\mathbf{h}_{d,k_t} + \mathbf{h}_{D,k_t}^t(t_{DT}))^H \mathbf{w}_{ZF,u} \right|^2 \right] + \delta^2} \right)}, \end{aligned} \quad (21)$$

and

$$\begin{aligned} R_{\text{sum}}^r &= \sum_{k_r \in \mathcal{K}_r} R_{k_r}^r = \sum_{k_r \in \mathcal{K}_r} \log_2(1 + \gamma_{k_r}^r) \\ &= \sum_{k_r \in \mathcal{K}_r} \log_2 \left(1 + \frac{\mathbb{E} \left[\left| (\mathbf{h}_{d,k_r} + \mathbf{h}_{D,k_r}^r(t_{DT}))^H \mathbf{w}_{ZF,k_r} \right|^2 \right]}{\mathbb{E} \left[\sum_{u \neq k_r} \left| (\mathbf{h}_{d,k_r} + \mathbf{h}_{D,k_r}^r(t_{DT}))^H \mathbf{w}_{ZF,u} \right|^2 \right] + \delta^2} \right)}, \end{aligned} \quad (22)$$

However, the achievable downlink rates given in (21) and (22) are implicit. To this end, more-explicit lower bounds of R_{sum}^t and R_{sum}^r are required. Therefore, we further derive the more useful lower bounds in the following Theorem 1 and Theorem 2. More specifically, the more-explicit lower bounds of R_{sum}^t and R_{sum}^r in Theorem 1 are derived based on the constant-amplitude IOS model.

Theorem 1: For a constant-amplitude DIOS, the lower bound on the ergodic achievable R&R sum rate R_{sum}^t and

R_{sum}^r converges in probability towards a fixed value as $N_D \rightarrow \infty$, i.e.,

$$R_{\text{sum}}^t \xrightarrow{P} \sum_{k_t \in \mathcal{K}_t} \log_2 \left(1 + \frac{\mathbb{E} \left[\frac{P_0}{\text{tr}(\mathbf{H}_d^H \mathbf{H}_d)^{-1}} \right] + \frac{P_0 \mathcal{L}_G \mathcal{L}_{1,k_t}^t N_D}{2K}}{\frac{P_0 \mathcal{L}_G (\sum_{u \neq k_t} \mathcal{L}_{1,u}) N_D}{2K} + \delta^2} \right) \quad (23)$$

$$\geq \sum_{k_t \in \mathcal{K}_t} \log_2 \left(1 + \frac{\frac{2P_0 K (N_A - K)}{\sum_{k=1}^K \frac{1}{\mathcal{L}_{d,k}}} + P_0 \mathcal{L}_G \mathcal{L}_{1,k_t}^t N_D}{P_0 \mathcal{L}_G (\sum_{u \neq k_t} \mathcal{L}_{1,u}) N_D + 2K \delta^2} \right) \quad (24)$$

and

$$R_{\text{sum}}^r \xrightarrow{P} \sum_{k_r \in \mathcal{K}_r} \log_2 \left(1 + \frac{\mathbb{E} \left[\frac{P_0}{\text{tr}(\mathbf{H}_d^H \mathbf{H}_d)^{-1}} \right] + \frac{P_0 \mathcal{L}_G \mathcal{L}_{1,k_r}^r N_D}{2K}}{\frac{P_0 \mathcal{L}_G (\sum_{u \neq k_r} \mathcal{L}_{1,u}) N_D}{2K} + \delta^2} \right) \quad (25)$$

$$\geq \sum_{k_r \in \mathcal{K}_r} \log_2 \left(1 + \frac{\frac{2K P_0 (N_A - K)}{\sum_{k=1}^K \frac{1}{\mathcal{L}_{d,k}}} + P_0 \mathcal{L}_G \mathcal{L}_{1,k_r}^r N_D}{P_0 \mathcal{L}_G (\sum_{u \neq k_r} \mathcal{L}_{1,u}) N_D + 2K \delta^2} \right) \quad (26)$$

Proof: Conditioned on the fact that the random variables \mathbf{h}_{d,k_t} , $\mathbf{h}_{D,k_t}^t(t_{DT})$, and \mathbf{w}_{ZF,k_t} are independent of each other, we can reduce numerator terms in (21) and (22) to the following forms:

$$\begin{aligned} & \mathbb{E} \left[\left| (\mathbf{h}_{d,k_t} + \mathbf{h}_{D,k_t}^t(t_{DT}))^H \mathbf{w}_{ZF,k_t} \right|^2 \right] \\ &= \mathbb{E} \left[\left| \mathbf{h}_{d,k_t}^H \mathbf{w}_{ZF,k_t} \right|^2 \right] + \mathbb{E} \left[\left| (\mathbf{h}_{D,k_t}^t(t_{DT}))^H \mathbf{w}_{ZF,k_t} \right|^2 \right] \end{aligned} \quad (27)$$

$$= \mathbb{E} \left[\frac{P_0}{\left\| \mathbf{H}_d (\mathbf{H}_d^H \mathbf{H}_d)^{-1} \right\|^2} \right] + \mathbb{E} \left[\left| (\mathbf{h}_{D,k_t}^t(t_{DT}))^H \mathbf{w}_{ZF,k_t} \right|^2 \right], \quad (28)$$

and

$$\begin{aligned} & \mathbb{E} \left[\left| (\mathbf{h}_{d,k_r} + \mathbf{h}_{D,k_r}^r(t_{DT}))^H \mathbf{w}_{ZF,k_r} \right|^2 \right] \\ &= \mathbb{E} \left[\left| \mathbf{h}_{d,k_r}^H \mathbf{w}_{ZF,k_r} \right|^2 \right] + \mathbb{E} \left[\left| (\mathbf{h}_{D,k_r}^r(t_{DT}))^H \mathbf{w}_{ZF,k_r} \right|^2 \right] \end{aligned} \quad (29)$$

$$= \mathbb{E} \left[\frac{P_0}{\left\| \mathbf{H}_d (\mathbf{H}_d^H \mathbf{H}_d)^{-1} \right\|^2} \right] + \mathbb{E} \left[\left| (\mathbf{h}_{D,k_r}^r(t_{DT}))^H \mathbf{w}_{ZF,k_r} \right|^2 \right]. \quad (30)$$

In (28) and (30), the expectations $\mathbb{E} \left[\left| (\mathbf{h}_{D,k_t}^t(t_{DT}))^H \mathbf{w}_{ZF,k_t} \right|^2 \right]$ and $\mathbb{E} \left[\left| (\mathbf{h}_{D,k_r}^r(t_{DT}))^H \mathbf{w}_{ZF,k_r} \right|^2 \right]$ can be reduced to

$$\begin{aligned} & \mathbb{E} \left[\left| (\mathbf{h}_{D,k_t}^t(t_{DT}))^H \mathbf{w}_{ZF,k_t} \right|^2 \right] \\ &= \sum_{n=1}^{N_A} \mathbb{E} \left[\left| [\mathbf{h}_{D,k_t}^t(t_{DT})]_n \right|^2 \right] \mathbb{E} \left[\left| [\mathbf{w}_{ZF,k_t}]_n \right|^2 \right], \end{aligned} \quad (31)$$

and

$$\begin{aligned} & \mathbb{E} \left[\left| (\mathbf{h}_{D,k_r}^r(t_{DT}))^H \mathbf{w}_{ZF,k_r} \right|^2 \right] \\ &= \sum_{n=1}^{N_A} \mathbb{E} \left[\left| [\mathbf{h}_{D,k_r}^r(t_{DT})]_n \right|^2 \right] \mathbb{E} \left[\left| [\mathbf{w}_{ZF,k_r}]_n \right|^2 \right], \end{aligned} \quad (32)$$

where $[\mathbf{h}_{D,k_t}^t(t_{DT})]_n$, $[\mathbf{w}_{ZF,k_t}]_n$, $[\mathbf{h}_{D,k_r}^r(t_{DT})]_n$, and $[\mathbf{w}_{ZF,k_r}]_n$ represent the n -th variables of $\mathbf{h}_{D,k_t}^t(t_{DT})$, \mathbf{w}_{ZF,k_t} , $\mathbf{h}_{D,k_r}^r(t_{DT})$, and \mathbf{w}_{ZF,k_r} , respectively.

Based on the statistical characteristics derived in Proposition 1, we have

$$\mathbb{E} \left[\left| (\mathbf{h}_{D,k_t}^t(t_{DT}))^H \mathbf{w}_{ZF,k_t} \right|^2 \right] \xrightarrow{P} \frac{\mathcal{L}_G \mathcal{L}_{1,k_t}^t N_D \mathbb{E} \left[\left\| \mathbf{w}_{ZF,k_t} \right\|^2 \right]}{2} \quad (33)$$

$$\xrightarrow{P} \frac{\mathcal{L}_G \mathcal{L}_{1,k_t}^t N_D P_0}{2K}, \quad (34)$$

and

$$\mathbb{E} \left[\left| (\mathbf{h}_{D,k_r}^r(t_{DT}))^H \mathbf{w}_{ZF,k_r} \right|^2 \right] \xrightarrow{P} \frac{\mathcal{L}_G \mathcal{L}_{1,k_r}^r N_D \mathbb{E} \left[\left\| \mathbf{w}_{ZF,k_r} \right\|^2 \right]}{2} \quad (35)$$

$$\xrightarrow{P} \frac{\mathcal{L}_G \mathcal{L}_{1,k_r}^r N_D P_0}{2K}, \quad (36)$$

as $N_D \rightarrow \infty$.

Moreover, we can reduce the term in (28) and (30) based on the Jensen inequality, i.e.,

$$\mathbb{E} \left[\frac{1}{\left\| \mathbf{H}_d (\mathbf{H}_d^H \mathbf{H}_d)^{-1} \right\|^2} \right] \geq \frac{1}{\mathbb{E} \left[\left\| \mathbf{H}_d (\mathbf{H}_d^H \mathbf{H}_d)^{-1} \right\|^2 \right]}. \quad (37)$$

Using an idiomatic trick that $\text{tr}(\mathbf{A}^H \mathbf{A}) = \|\mathbf{A}\|^2$, we can obtain that

$$\mathbb{E} \left[\left\| \mathbf{H}_d (\mathbf{H}_d^H \mathbf{H}_d)^{-1} \right\|^2 \right] = \mathbb{E} \left[\text{tr} \left((\mathbf{H}_d^H \mathbf{H}_d)^{-1} \right) \right]. \quad (38)$$

Based on the channel model of \mathbf{H}_d in (16), we further reduce (38) to

$$\mathbb{E} \left[\text{tr} \left((\mathbf{H}_d^H \mathbf{H}_d)^{-1} \right) \right] = \mathbb{E} \left[\text{tr} \left(\mathbf{\Lambda}^{-1} (\widehat{\mathbf{H}}_d^H \widehat{\mathbf{H}}_d)^{-1} \right) \right], \quad (39)$$

where $\mathbf{\Lambda} = \text{diag}(\mathcal{L}_{d,1}, \mathcal{L}_{d,2}, \dots, \mathcal{L}_{d,K})$ and $\widehat{\mathbf{H}}_d = [\widehat{\mathbf{h}}_{d,1}, \widehat{\mathbf{h}}_{d,2}, \dots, \widehat{\mathbf{h}}_{d,K}]$. Consequently, $\widehat{\mathbf{H}}_d^H \widehat{\mathbf{H}}_d$ is a central complex Wishart matrix.

Exploiting the property of complex Wishart matrices [42], we can further reduce (38) to the following form:

$$\mathbb{E} \left[\text{tr}(\mathbf{H}_d^H \mathbf{H}_d)^{-1} \right] = \frac{1}{N_A - K} \sum_{k=1}^K \frac{1}{\mathcal{L}_{d,k}}. \quad (40)$$

As a result, we can obtain the following inequalities:

$$\begin{aligned} & \mathbb{E} \left[\left| (\mathbf{h}_{d,k_t} + \mathbf{h}_{D,k_t}^t(t_{DT}))^H \mathbf{w}_{ZF,k_t} \right|^2 \right] \geq \\ & \frac{P_0 (N_A - K)}{\sum_{k=1}^K \frac{1}{\mathcal{L}_{d,k}}} + \frac{P_0 \mathcal{L}_G \mathcal{L}_{1,k_t}^t N_D}{2K}, \end{aligned} \quad (41)$$

and

$$\mathbb{E} \left[\left| (\mathbf{h}_{d,k_r} + \mathbf{h}_{D,k_r}^r(t_{DT}))^H \mathbf{w}_{ZF,k_r} \right|^2 \right] \geq \frac{P_0(N_A - K)}{\sum_{k=1}^K \frac{1}{\mathcal{L}_{d,k}}} + \frac{P_0 \mathcal{L}_G \mathcal{L}_{I,k_r}^r N_D}{2K}, \quad (42)$$

Moreover, similar to the derivations in (34) and (36), we can directly reduce the expectations in the denominators expressed in (21) and (22) to

$$\mathbb{E} \left[\sum_{u \neq k_t} \left| (\mathbf{h}_{D,k_t}^t(t_{DT}))^H \mathbf{w}_{ZF,u} \right|^2 \right] \xrightarrow{P} \frac{P_0 \mathcal{L}_G \left(\sum_{u \neq k_t} \mathcal{L}_{I,u} \right) N_D}{2K}, \quad (43)$$

and

$$\mathbb{E} \left[\sum_{u \neq k_r} \left| (\mathbf{h}_{D,k_r}^r(t_{DT}))^H \mathbf{w}_{ZF,u} \right|^2 \right] \xrightarrow{P} \frac{P_0 \mathcal{L}_G \left(\sum_{u \neq k_r} \mathcal{L}_{I,u} \right) N_D}{2K}. \quad (44)$$

Combining the formulations from (41) to (44), we can obtain Theorem 1. ■

Moreover, the more-explicit lower bounds of R_{sum}^t and R_{sum}^r in Theorem 2 are derived based on the variable-amplitude IOS model.

Theorem 2: For a variable-amplitude DIOS, the lower bound on the ergodic achievable R&R sum rate R_{sum}^t and R_{sum}^r converges in probability towards a fixed value as $N_D \rightarrow \infty$, i.e.,

$$\begin{aligned} R_{\text{sum}}^t &\xrightarrow{P} \sum_{k_t \in \mathcal{K}_t} \log_2 \left(1 + \frac{\mathbb{E} \left[\frac{P_0}{\text{tr}(\mathbf{H}_d^H \mathbf{H}_d)} \right] + \frac{P_0 \mathcal{L}_G \mathcal{L}_{I,k_t}^t N_D \mu}{K}}{P_0 \mathcal{L}_G \left(\sum_{u \neq k_t} \mathcal{L}_{I,u} \right) N_D \mu + \delta^2} \right) \\ &\geq \sum_{k_t \in \mathcal{K}_t} \log_2 \left(1 + \frac{\frac{P_0 K (N_A - K)}{\sum_{k=1}^K \frac{1}{\mathcal{L}_{d,k}}} + P_0 \mathcal{L}_G \mathcal{L}_{I,k_t}^t N_D \mu}{P_0 \mathcal{L}_G \left(\sum_{u \neq k_t} \mathcal{L}_{I,u} \right) N_D \mu + K \delta^2} \right), \end{aligned} \quad (45)$$

and

$$\begin{aligned} R_{\text{sum}}^r &\xrightarrow{P} \sum_{k_r \in \mathcal{K}_r} \log_2 \left(1 + \frac{\mathbb{E} \left[\frac{P_0}{\text{tr}(\mathbf{H}_d^H \mathbf{H}_d)} \right] + \frac{P_0 \mathcal{L}_G \mathcal{L}_{I,k_r}^r N_D (1-\mu) N_A}{K}}{P_0 \mathcal{L}_G \left(\sum_{u \neq k_r} \mathcal{L}_{I,u} \right) N_D (1-\mu) + \delta^2} \right) \\ &\geq \sum_{k_r \in \mathcal{K}_r} \log_2 \left(1 + \frac{\frac{P_0 K (N_A - K)}{\sum_{k=1}^K \frac{1}{\mathcal{L}_{d,k}}} + P_0 \mathcal{L}_G \mathcal{L}_{I,k_r}^r N_D (1-\mu) N_A}{P_0 \mathcal{L}_G \left(\sum_{u \neq k_r} \mathcal{L}_{I,u} \right) N_D (1-\mu) + K \delta^2} \right). \end{aligned} \quad (46)$$

Proof: The proof of Theorem 2 is similar to those of Theorem 1. The main difference, however, concerns the expectations of the absolute value squareds of $(\mathbf{h}_{D,k_t}^t(t_{DT}))^H \mathbf{w}_{ZF,k_t}$ and $(\mathbf{h}_{D,k_r}^r(t_{DT}))^H \mathbf{w}_{ZF,k_r}$ expressed in (34) and (36). More specifically, based on the statistical characteristics derived in

TABLE II
A ONE-BIT DIOS WITH VARIABLE AMPLITUDES

Index	θ_m^r	ξ_m^r	θ_m^t	ξ_m^t	P_m
$m = 1$	$\pi/9$	0.62	$5\pi/3$	0.78	0.25
$m = 2$	$7\pi/6$	0.57	$2\pi/3$	0.82	0.75

Proposition 2, the expectations of $\|(\mathbf{h}_{D,k_t}^t(t_{DT}))^H \mathbf{w}_{ZF,k_t}\|^2$ and $\|(\mathbf{h}_{D,k_r}^r(t_{DT}))^H \mathbf{w}_{ZF,k_r}\|^2$ are given by

$$\begin{aligned} \mathbb{E} \left[\left| (\mathbf{h}_{D,k_t}^t(t_{DT}))^H \mathbf{w}_{ZF,k_t} \right|^2 \right] &\xrightarrow{P} \mathcal{L}_G \mathcal{L}_{I,k_t}^t N_D \mu \mathbb{E} \left[\|\mathbf{w}_{ZF,k_t}\|^2 \right] \\ &\xrightarrow{P} \frac{\mathcal{L}_G \mathcal{L}_{I,k_t}^t N_D \mu P_0}{K}, \end{aligned} \quad (49)$$

and

$$\mathbb{E} \left[\left| (\mathbf{h}_{D,k_r}^r(t_{DT}))^H \mathbf{w}_{ZF,k_r} \right|^2 \right] \xrightarrow{P} \mathcal{L}_G \mathcal{L}_{I,k_r}^r N_D (1-\mu) \mathbb{E} \left[\|\mathbf{w}_{ZF,k_r}\|^2 \right] \quad (50)$$

$$\xrightarrow{P} \frac{\mathcal{L}_G \mathcal{L}_{I,k_r}^r N_D (1-\mu) P_0}{K}, \quad (51)$$

as $N_D \rightarrow \infty$. ■

From Theorem 1, one can see that the omnidirectional jamming impacts of the DIOS-based FPJ refractive-side LUs and reflective-side LUs are independent on the quantization bits and the distribution of the DIOS coefficients. According to (24) and (26), the jamming impact is related to the element number of the DIOS. However, based on Theorem 2, one can see that the jamming impact depends on statistical parameter μ . Namely, the possible amplitude values of each DIOS element and the distribution of the DIOS amplitudes (i.e., the quantization bits and the distribution of DIOS phase shifts). It can be seen that from (46) and (48) the jamming impacts on the refractive-side LUs and the reflective-side LUs can be tuned by adjusting μ , i.e., the quantization bits and the distribution of the DIOS coefficients. Therefore, we can design a appropriate distribution to balance the impacts of the DIOS-based omnidirectional fully-passive jamming attacks on the refractive-side LUs and the reflective-side LUs.

IV. SIMULATION RESULTS AND DISCUSSION

In this section, we present numerical results to show the impact of the proposed DIOS-based FPJ. We consider an MU-MISO system, where a legitimate AP is equipped with 128-element antenna array to communicate with 24 single-antenna LUs, i.e., $N_A = 128$ and $K = 24$. Furthermore, the AP is assumed to be located at (0m, 0m, 10m) and the R&R LUs are randomly distributed in the circular region \mathcal{S} centered at (0m, 180m, 0m) with a radius of 20m. In addition, a one-bit DIOS (i.e., $b = 1$) with 2,048 elements ($N_D = 2,048$) is deployed at (2m, 2m, 8m) to implement fully-passive jamming to attack these LUs. Without loss of generality, we assume that these LUs are uniformly distributed in \mathcal{S} , with half of them on the refractive-side of the DIOS and the other half on the reflective-side of the DIOS.

For the DIOS with variable amplitudes, its R&R coefficients are given in Table II [33]. For the DIOS with the constant amplitude, we assume that the R&R phase shifts are the same to those in Table II, while the amplitude is $\frac{\sqrt{2}}{2}$. Furthermore,

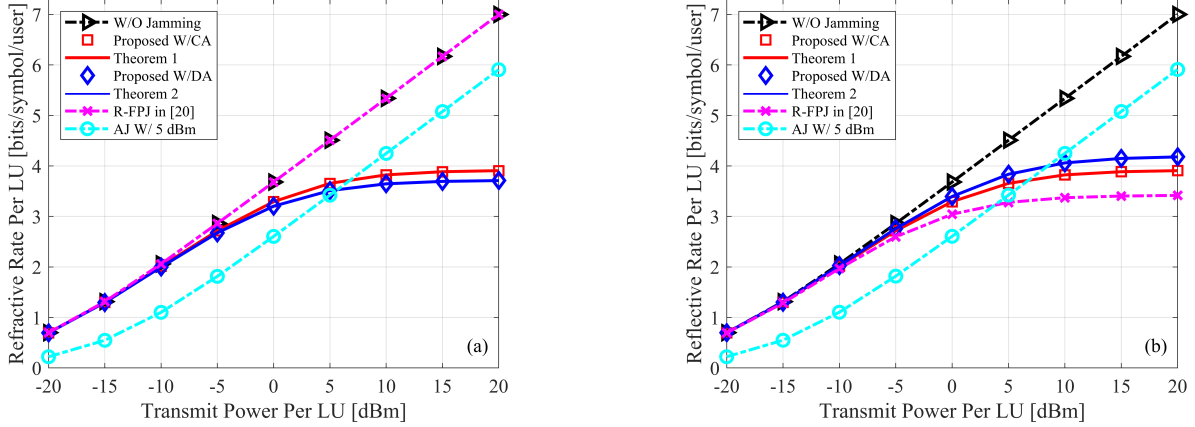


Fig. 2. Achievable performance of (a) refractive-side LUs and (b) reflective-side LUs vs transmit power for different benchmarks.

the probabilities of taking θ_1^t and θ_2^t are 0.25 and 0.75. As a result, μ in Theorem 2 is computed as 0.66. Moreover, we assume that the length of the DT phase is six times of that of the RPT phase, i.e., $C = 6$.

According to the 3GPP propagation model [43], the propagation parameters of the wireless channels modeled in Section II-B are described as follows: $\mathcal{L}_G = 35.6 + 22\log_{10}(d_i)$ and $\mathcal{L}_{1,k}^t, \mathcal{L}_{1,k}^r, \mathcal{L}_{d,k} = 32.6 + 36.7\log_{10}(d_i)$, where d_i is the propagation distance. Moreover, the AWGN variance is $\delta^2 = -170 + 10\log_{10}(BW)$ dBm, and $BW = 180$ kHz. If not otherwise specified, these above parameters default to the values.

Fig. 2 shows the downlink rate per LU versus $(\frac{R_{\text{sum}}}{K})$ the transmit power per LU ($\frac{P_0}{K}$) from different schemes. Specifically, the performance of the following benchmarks is considered and compared: 1) the sum rate per LU without jamming attacks (W/O Jamming); 2) the sum rate per LU jammed by the proposed DIOS-based FPJ using the constant-amplitude IOS model (Proposed W/ CA) and 3) the corresponding theoretical analysis in Theorem 1 (Theorem 1); 4) the sum rate per LU jammed by the proposed DIOS-based FPJ using the variable-amplitude IOS model (Proposed W/ VA) and 5) the corresponding theoretical analysis in Theorem 2 (Theorem 2); 6) the sum rate per LU jammed by the reflective DRIS-based FPJ in [20] (R-FPJ in [20]); 7) the sum rate per LU jammed by an AJ emitting 5 dBm jamming power (AJ W/ 5 dBm). In addition, Fig. 2 (a) illustrates the achievable performance of the refractive-side LUs via the above benchmarks, and Fig. 2 (b) illustrates the achievable performance of the reflective-side LUs.

From Fig. 2, it can be seen that the reflective DRIS-based FPJ [20], [21] jams the reflective-side LUs, but does not jam the refractive-side LUs. One can see that the achievable sum rate per LU of the refractive-side LUs does not decrease when attacked by the reflective DRIS-based FPJ. However, the proposed DIOS-based FPJ can jam both the refractive-side LUs and the reflective-side LUs. The reflective DRIS-based FPJ can achieve more severe jamming impact on the reflective-side LUs. However, the average performance loss

per LU jammed by the proposed DIOS-based FPJ is 1.5091 bits/symbol/user at 10 dBm transmit power per LU, while that caused by the DRIS-based FPJ is only 0.9746 bits/symbol/user. In other words, the proposed DIOS-based FPJ can not only perform 360° fully-passive jamming, but also improve the jamming impact by about 55% at 10dBm transmit power per legitimate user. Moreover, as stated above, μ in Theorem 2 is 0.66 based on the settings in Table II. As a result, one can see that the jamming impact of the proposed DIOS-based FPJ on the refractive-side LUs is more significant than that on the reflective-side LUs. It is worth noting that the can change the random distribution of the DIOS phase shifts to balance the jamming effects between the refractive-side LUs and the reflective-side LUs.

Compared to the jamming impact of an AJ, the jamming impact of the proposed DIOS-based FPJ can not be suppressed by increasing the transmit power at the legitimate AP. As shown in Fig. 2, as the transmit power per LU increases, the jamming impact of the proposed DIOS-based FPJ increases and eventually surpasses that of the AJ. Moreover, Fig. 2 also verifies the validity of the derived Theorem 1 and Theorem 2. It can be seen that the results of the asymptotic analysis provided in Theorem 1 and Theorem 2 are very close to the downlink rates obtained using Monte Carlo simulation.

Fig. 3 illustrates the relationship between the achievable performance and the number of the DIOS elements. The jamming impacts of the proposed DIOS-based FPJ on both the refractive-side LUs and the reflective-side LUs increase with the number of the DIOS elements. From Theorem 1 and Theorem 2, it can also be seen that the omnidirectional fully-passive jamming impact is caused by ACA interference, which is related to the number of the DIOS elements, i.e., N_D . Note that the proposed DIOS-based FPJ in our paper is implemented by using only 1-bit quantization DIOS phase shifts. Therefore, it is easy to implement the proposed DIOS-based FPJ and then increase its omnidirectional jamming impact by using a larger number of the DIOS elements. Although the proposed DIOS-based FPJ

For the refractive-side LUs, the proposed DIOS-based FPJ

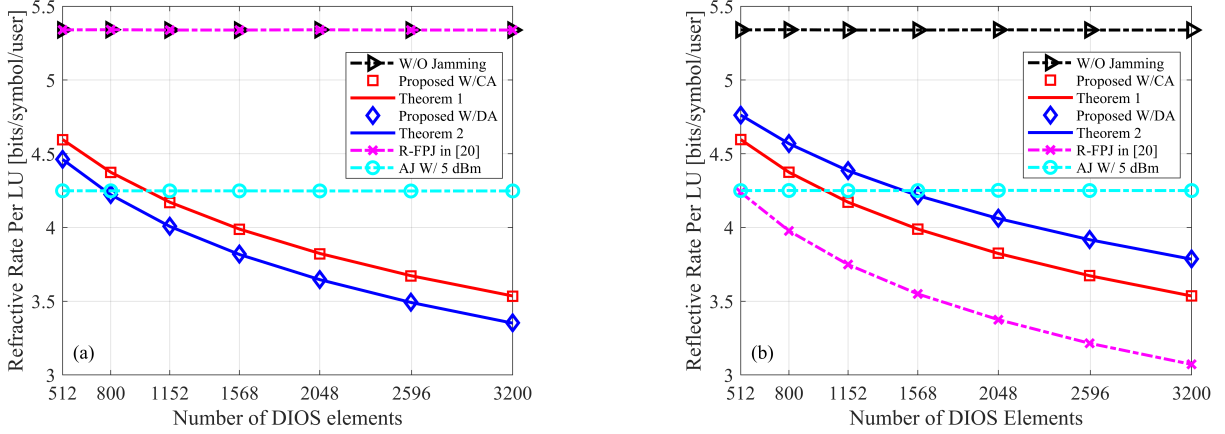


Fig. 3. Achievable performance of (a) refractive-side LUs and (b) reflective-side LUs vs the number of the DIOS elements at 10 dBm transmit power per LU for different benchmarks.

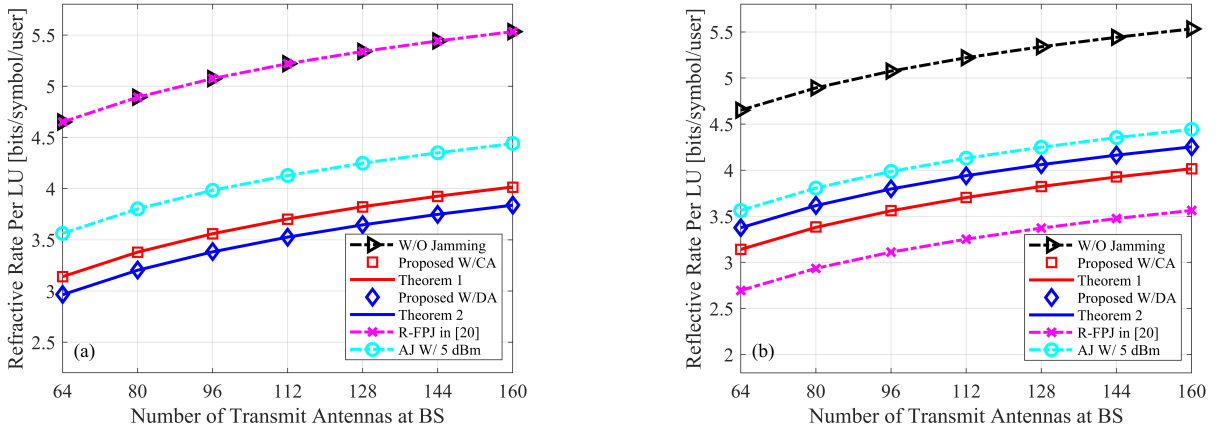


Fig. 4. Achievable performance of (a) refractive-side LUs and (b) reflective-side LUs vs the number of transmit antennas at 10 dBm transmit power per LU for different benchmarks.

implemented by the constant-amplitude DIOS can achieve the same jamming impact as the AJ with 5 dBm jamming power when the number of DIOS elements is about 1,000. Meanwhile, when the DIOS-based FPJ is implemented by the variable-amplitude DIOS, it is enough to achieve the same jamming impact as the AJ with 5 dBm jamming power as the number of DIOS elements is about 800. This is because that the μ in Theorem 2 is equal to 0.66 for the refractive-side LUs, while it is regarded as 0.5 in Theorem 1. As a result, the DIOS-based FPJ implemented by a variable-amplitude DIOS launches more severe fully-passive jamming on the refractive-side LUs. However, for the reflective-side LUs, the DIOS-based FPJ implemented by the variable-amplitude DIOS achieves the same jamming impact as the AJ with 5 dBm jamming power, while the number of the DIOS elements required is 1,568. This is because that $(1 - \mu)$ is equal to 0.34 in the Theorem 2. As a result, the jamming impact of the DIOS-based FPJ implemented by the variable-amplitude DIOS is weaker than that of the DIOS-based FPJ implemented by the constant-amplitude DIOS.

Fig. 4 shows the performance of different benchmarks as a function of the number of transmit antennas at 10 dBm transmit power per LU. It can be seen that the achievable sum rates per LU for both the refractive-side LUs and the reflective-side LUs improve as the number of transmit antennas increases. In fact, it is clear from Theorem 1 and Theorem 2 that the omnidirectional fully-passive jamming attacks can be suppressed by increasing N_A , which suggests that one possible scheme to mitigate the DIOS-based 360° fully-passive jamming is to use a larger number of transmit antennas at the AP. Unfortunately, the more transmit antennas a base station has, the higher the implementation cost becomes.

Moreover, the relationship between the performance obtained from the corresponding benchmarks and the number of the AP transmit antennas, while the number of DIOS elements also increases with the number of the transmit antennas. Specifically, the number of the DIOS is always equal to the 16 times of the number of the transmit antennas, i.e., $N_D = 16N_A$. As shown in Fig. 5, an attacker can use a larger number of DIOS elements to counteract the mitigation provided by the

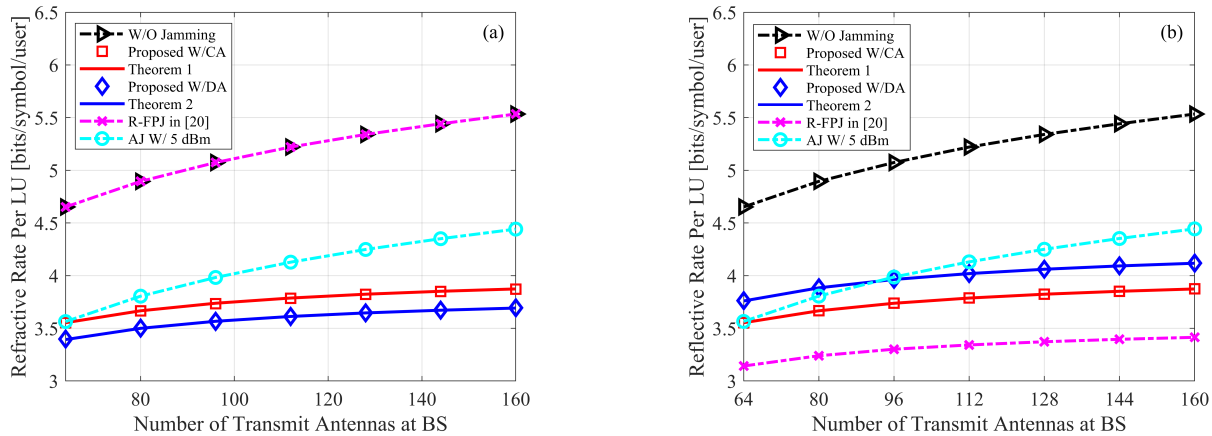


Fig. 5. Achievable performance of (a) refractive-side LUs and (b) reflective-side LUs vs the number of transmit antennas at 10 dBm transmit power per LU for different benchmarks, where the number of the DIOS is always equal to the 16 times of the number of transmit antennas.

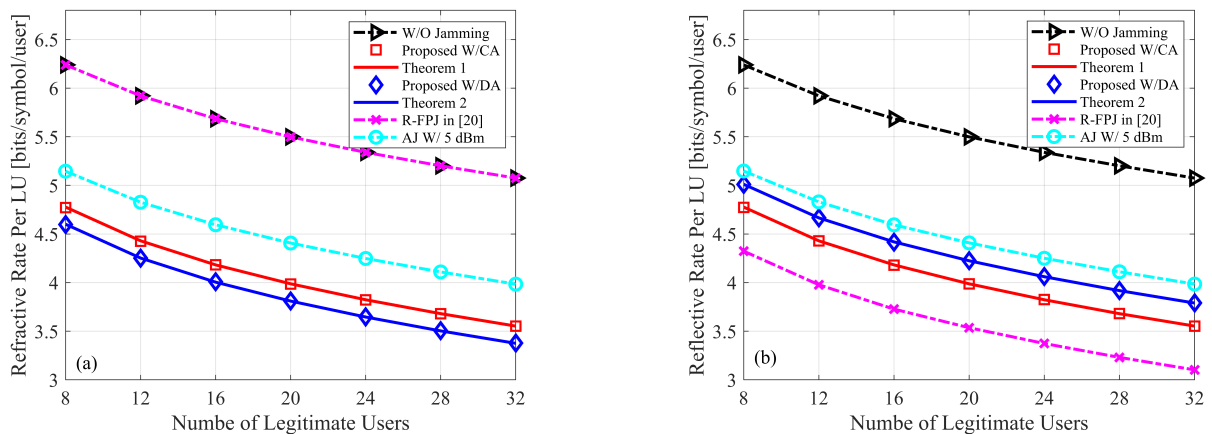


Fig. 6. Achievable performance of (a) refractive-side LUs and (b) reflective-side LUs vs the number of the LUs at 10 dBm transmit power per LU for different benchmarks.

increase in the AP transmit antennas. It is worth noting that the proposed DIOS-based FPJ can be implemented by using 1-bit quantization IOS, which ensures that the implementation of increasing the number of DIOS elements is cheaper compared to that of increasing the number of the transmit antennas. Note that the traditional anti-jamming technologies, such as frequency hopping, are ineffective against the proposed DIOS-based FPJ [21].

Fig. 6 shows the relationship between the achievable performance via different benchmarks and the number of the LUs. On the one hand, increasing the number of LUs reduces the gain generated by the transmit precoding at the . On the other hand, the greater the number of LUs, the greater the ACA interference caused by the DIOS. As a result, one can see that the omnidirectional fully-passive jamming impact becomes more severe as the number of the LUs increases. In future scenarios of ultra-massive user access in 6G, the proposed DIOS-based FPJ poses a serious potential threat, particularly when the number of legitimate users (LUs) is extremely large. Therefore, it is necessary for the legitimate AP to investigate

other more cost-effective anti-jamming solutions, for instance, the anti-jamming precoding [44], [45].

V. CONCLUSIONS

In this work, we proposed a DIOS-based FPJ to launch 360° fully-passive jamming attacks on MU-MISO systems. Unlike existing AJs and RIS-based PJs, the proposed DIOS-based FPJ leverages ACA interference to launch omnidirectional fully-passive jamming attacks. As a result, the DIOS-based FPJ operates without requiring neither jamming power nor LU channel knowledge. To characterize the impact of the DIOS-based FPJ on the MU-MISO system, we first derived the statistical characteristics of the DIOS-jammed channels based on the two considered IOS model. Then, a lower bound of the achievable sum rates under the constant-amplitude DIOS and variable-amplitude DIOS assumptions are obtained based on the derived statistical characteristics.

The following properties are resulted from the theoretical derivations: 1) The omnidirectional jamming impact of

the proposed DIOS-based FPJ implemented by a constant-amplitude IOS does not depend on neither the quantization number nor the stochastic distribution of the DIOS coefficients; 2) However, the omnidirectional jamming impact of the proposed DIOS-based FPJ depends on the quantization bits and the stochastic distribution of the DIOS coefficients when the variable-amplitude DIOS is used. Therefore, we can use a variable-amplitude DIOS and carefully design a DIOS coefficient distribution to balance the jamming impacts on the refractive-side LUs and the reflective-side LUs.

The proposed DIOS-based FPJ can not only launch 360° fully-passive jamming attacks, but also achieves a more severe jamming impact compared to the existing DRIS-based FPJ. Increasing the transmit power at the AP does not mitigate the omnidirectional jamming attacks initiated by the proposed DIOS-based FPJ; Instead, it exacerbates the jamming impact. In addition, the DIOS-based FPJ can effectively evade conventional anti-jamming techniques, including frequency hopping. Although the APs can mitigate the proposed DIOS-based omnidirectional fully-passive jamming attacks by increasing its transmit antennas, this countermeasure becomes less effective as the number of DIOS elements increases.

APPENDIX A PROOF OF PROPOSITION 1

Based on the definition of $\mathbf{H}_D^t(t)$, the element $[\mathbf{H}_D^t(t)]_{n,k_t}$ is written as

$$\begin{aligned} [\mathbf{H}_D^t(t)]_{n,k_t} = & \sqrt{\frac{\varepsilon_G \mathcal{L}_G \mathcal{L}_{I,k_t}^t N_D}{1 + \varepsilon_G}} \left(\frac{\sum_{s=1}^{N_D} [\hat{\mathbf{h}}_{1,k_t}^t]_s \alpha_s^t(t) e^{j\varphi_s^t(t)}}{\sqrt{N_D}} \right. \\ & \times e^{-j\frac{2\pi}{\lambda}(d_{n,s} - d_n)} + \sqrt{\frac{\mathcal{L}_G \mathcal{L}_{I,k_t}^r N_D}{1 + \varepsilon_G}} \left(\frac{\sum_{s=1}^{N_D} [\hat{\mathbf{h}}_{1,k_t}^t]_s}{\sqrt{N_D}} \right. \\ & \left. \left. \times \alpha_s^t(t) e^{j\varphi_s^t(t)} [\hat{\mathbf{G}}^{\text{NLOS}}]_{n,s} \right) \right), \end{aligned} \quad (53)$$

where $[\hat{\mathbf{h}}_{1,k}]_s$ represents the s -th element of $\hat{\mathbf{h}}_{1,k}$ in (14). Conditioned on the fact that the i.i.d. elements of $\mathbf{H}_I^t(t)$, $\varphi_t(t)$, and \mathbf{G} are independent, we have

$$\begin{aligned} \mathbb{E}[a_s^t] &= \mathbb{E}\left[\left[\hat{\mathbf{h}}_{1,k_t}^t\right]_s \alpha_s^t(t) e^{j\varphi_s^t(t)} e^{-j\frac{2\pi}{\lambda}(d_{n,s} - d_n)}\right] \\ &= \mathbb{E}\left[\left[\hat{\mathbf{h}}_{1,k_t}^t\right]_s\right] \mathbb{E}\left[\alpha_s^t(t) e^{j\varphi_s^t(t)} e^{-j\frac{2\pi}{\lambda}(d_{n,s} - d_n)}\right] = 0, \end{aligned} \quad (54)$$

and

$$\begin{aligned} \mathbb{E}[b_s^t] &= \mathbb{E}\left[\left[\hat{\mathbf{h}}_{1,k_t}^t\right]_s \alpha_s^t(t) e^{j\varphi_s^t(t)} [\hat{\mathbf{G}}^{\text{NLOS}}]_{n,s}\right] \\ &= \mathbb{E}\left[\left[\hat{\mathbf{h}}_{1,k_t}^t\right]_s\right] \mathbb{E}\left[\alpha_s^t(t) e^{j\varphi_s^t(t)} [\hat{\mathbf{G}}^{\text{NLOS}}]_{n,s}\right] = 0, \end{aligned} \quad (55)$$

where $s = 1, 2, \dots, N_D$. Since the amplitude $\alpha_s^t(t), \forall s$ is assumed to be constant and equal to $\frac{\sqrt{2}}{2}$, the variances of a_s^t and b_s^t are formulated as follows:

$$\text{Var}[a_s^t] = \frac{1}{2} \mathbb{E}\left[\left|[\hat{\mathbf{h}}_{1,k_t}^t]_s\right|^2\right] = \frac{1}{2}, \quad (56)$$

and

$$\text{Var}[b_s^t] = \frac{1}{2} \mathbb{E}\left[\left|[\hat{\mathbf{h}}_{1,k_t}^t]_s\right|^2\right] \mathbb{E}\left[\left|[\hat{\mathbf{G}}^{\text{NLOS}}]_{n,s}\right|^2\right] \quad (57)$$

$$= \frac{1}{2}. \quad (58)$$

According to the Lindeberg-Lévy central limit theorem, the random variables $\sum_{s=1}^{N_D} \frac{a_s^t}{\sqrt{N_D}}$ and $\sum_{s=1}^{N_D} \frac{b_s^t}{\sqrt{N_D}}$ in (53) converge in distribution to a normal distribution $\mathcal{CN}(0, \frac{1}{2})$ as $N_D \rightarrow \infty$, i.e.,

$$\sum_{s=1}^{N_D} \frac{a_s^t}{\sqrt{N_D}} \xrightarrow{d} \mathcal{CN}\left(0, \frac{1}{2}\right), \quad (59)$$

and

$$\sum_{s=1}^{N_D} \frac{b_s^t}{\sqrt{N_D}} \xrightarrow{d} \mathcal{CN}\left(0, \frac{1}{2}\right). \quad (60)$$

Consequently, (53) converges in distribution to the following distribution:

$$[\mathbf{H}_D^t(t)]_{n,k_t} \xrightarrow{d} \mathcal{CN}\left(0, \frac{\mathcal{L}_G \mathcal{L}_{I,k_t}^t N_D}{2}\right). \quad (61)$$

Similar to the derivation from (53) to (61), we have

$$[\mathbf{H}_D^r(t)]_{n,k_r} \xrightarrow{d} \mathcal{CN}\left(0, \frac{\mathcal{L}_G \mathcal{L}_{I,k_r}^r N_D}{2}\right). \quad (62)$$

APPENDIX B PROOF OF PROPOSITION 2

When we consider a more practical IOS model with variable amplitudes, the expectations in (54) and (55) also hold on. However, the variance in (56) is then reduced to

$$\text{Var}[a_s^t] = \mathbb{E}\left[\left|[\hat{\mathbf{h}}_{1,k_t}^t]_s\right|^2\right] \mathbb{E}\left[\alpha_s^t(t)^2\right]. \quad (63)$$

Furthermore,

$$\mathbb{E}\left[\alpha_s^t(t)^2\right] = \sum_{m=1}^{2^b} P_m(\xi_m^t)^2 = \mu. \quad (64)$$

Consequently, (63) is reduced to

$$\text{Var}[a_s^t] = \mu \mathbb{E}\left[\left|[\hat{\mathbf{h}}_{1,k_t}^t]_s\right|^2\right] = \mu. \quad (65)$$

Similarly,

$$\begin{aligned} \text{Var}[b_s^t] &= \mathbb{E}\left[\left|[\hat{\mathbf{h}}_{1,k_t}^t]_s\right|^2\right] \mathbb{E}\left[\alpha_s^t(t)^2\right] \mathbb{E}\left[\left|[\hat{\mathbf{G}}^{\text{NLOS}}]_{n,s}\right|^2\right] \\ &= \mu. \end{aligned} \quad (66)$$

Based on the Lindeberg-Lévy central limit theorem, the element $[\mathbf{H}_D^t(t)]_{n,k_t}$ converges to the following normal distribution as N_D , i.e.,

$$[\mathbf{H}_D^t(t)]_{n,k_t} \xrightarrow{d} \mathcal{CN}(0, \mathcal{L}_G \mathcal{L}_{1,k_t}^t N_D \mu). \quad (67)$$

Moreover, for the DIOS-jammed channels of the reflective-side LUs, the element $[\mathbf{H}_D^r(t)]_{n,k_r}$ transfers to

$$\begin{aligned} [\mathbf{H}_D^r(t)]_{n,k_r} = & \sqrt{\frac{\varepsilon_G \mathcal{L}_G \mathcal{L}_{1,k_r}^r N_D}{1 + \varepsilon_G}} \left(\frac{\sum_{s=1}^{N_D} [\hat{\mathbf{h}}_{1,k_r}^r]_s \alpha_s^r(t) e^{j\varphi_s^r(t)}}{\sqrt{N_D}} \right. \\ & \times e^{-j\frac{2\pi}{\lambda}(d_{n,s} - d_n)} + \sqrt{\frac{\mathcal{L}_G \mathcal{L}_{1,k_r}^r N_D}{1 + \varepsilon_G}} \left(\frac{\sum_{s=1}^{N_D} [\hat{\mathbf{h}}_{1,k_r}^r]_s}{\sqrt{N_D}} \right. \\ & \left. \left. \times \alpha_s^r(t) e^{j\varphi_s^r(t)} [\hat{\mathbf{G}}^{\text{NLOS}}]_{n,s} \right) \right), \quad (68) \end{aligned}$$

Consequently, the following random variables a_s^r and b_s^r can be defined, which are

$$a_s^r = [\hat{\mathbf{h}}_{1,k_r}^r(t)]_s \alpha_s^r(t) e^{j\varphi_s^r(t)} e^{-j\frac{2\pi}{\lambda}(d_{n,s} - d_n)}, \quad (69)$$

$$b_s^r = [\hat{\mathbf{h}}_{1,k_r}^r(t)]_s \alpha_s^r(t) e^{j\varphi_s^r(t)} [\hat{\mathbf{G}}^{\text{NLOS}}]_{n,s}. \quad (70)$$

Similar to the derivations of (65) and (66), the variances of a_s^r and b_s^r is written as

$$\text{Var}[a_s^r] = \text{Var}[b_s^r] = \mathbb{E} \left[\alpha_s^r(t) (\alpha_s^r(t))^H \right] = \sum_{m=1}^{2^b} P_m (\xi_m^r)^2. \quad (71)$$

Note that, due to the energy constraint of an IOS, we have $(\xi_m^r)^2 = 1 - (\xi_m^t)^2, \forall m$. Therefore, (71) reduces to

$$\text{Var}[a_s^r] = \text{Var}[b_s^r] = 1 - \mu. \quad (72)$$

Based on the Lindeberg-Lévy central limit theorem, the element $[\mathbf{H}_D^r(t)]_{n,k_r}$ follows a normal distribution. Specifically,

$$[\mathbf{H}_D^r(t)]_{n,k_r} \xrightarrow{d} \mathcal{CN}(0, \mathcal{L}_G \mathcal{L}_{1,k_r}^r N_D (1 - \mu)). \quad (73)$$

REFERENCES

- [1] Y. Zhang, H. Huang, H. Zhang, B. Di, W. Mei, J. Yuan, Y. Cai, "Disco intelligent omni-surface based fully-passive jamming attacks," in *Proc. IEEE/CIC Int. Commun. Conf. China (ICCC)*, Hangzhou, China, Aug. 2024.
- [2] A. Mukherjee, S. A. A. Fakoorian, J. Huang, and A. L. Swindlehurst, "Principles of physical layer security in multiuser wireless networks: A survey," *IEEE Commun. Surv. Tut.*, vol. 16, no. 3, pp. 1550–1573, 3rd Quarter 2014.
- [3] Y. Zou, J. Zhu, X. Wang, and L. Hanzo, "A survey on wireless security: Technical challenges, recent advances, and future trends," *Proceedings of the IEEE*, vol. 104, no. 9, pp. 1727–1765, Sep. 2016.
- [4] H. Pirayesh and H. Zeng, "Jamming attacks and anti-jamming strategies in wireless networks: A comprehensive survey," *IEEE Commun. Surv. Tut.*, vol. 24, no. 2, pp. 767–809, 2nd Quarter 2022.
- [5] O. Besson, P. Stoica, and Y. Kamiya, "Direction finding in the presence of an intermittent interference," *IEEE Trans. Signal Process.*, vol. 50, no. 7, pp. 1554–1564, Jul. 2002.
- [6] E. Lance and G. K. Kaleh, "A diversity scheme for a phase-coherent frequency-hopping spread-spectrum system," *IEEE Trans. Commun.*, vol. 45, no. 9, pp. 1123–1129, Sep. 1997.
- [7] J. Jeung, S. Jeong, and J. Lim, "Adaptive rapid channel-hopping scheme mitigating smart jammer attacks in secure WLAN," in *Proc. Military Commun. Conf.*, Baltimore, MD, Nov. 2011, pp. 1231–1236.
- [8] T. Cui, M. Qi, X. Wan, J. Zhao, and Q. Cheng, "Coding metamaterials, digital metamaterials and programmable metamaterials," *Light-Sci. Appl.*, vol. 3, e218, Oct. 2014.
- [9] Q. Wu and R. Zhang, "Towards smart and reconfigurable environment: Intelligent reflecting surface aided wireless network," *IEEE Commun. Mag.*, vol. 58, no. 1, pp. 106–112, Nov. 2021.
- [10] W. Mei, B. Zheng, C. You, and R. Zhang, "Intelligent reflecting surface aided wireless networks: From single-reflection to multi-reflection design and optimization," *Proc. IEEE*, vol. 110, no. 9, pp. 1380–1400, Sep. 2022.
- [11] H. Huang, Y. Zhang, H. Zhang, Z. Zhao, C. Zhang, and Z. Han, "Multi-IRS-aided millimeter-wave multi-user MISO systems for power minimization using generalized Benders decomposition," *IEEE Trans. Wireless Commun.*, vol. 22, no. 11, pp. 7873–7886, Mar. 2023.
- [12] C. Huang, A. Zappone, G. C. Alexandropoulos, M. Debbah, C. Yuen, "Reconfigurable intelligent surfaces for energy efficiency in wireless communication," *IEEE Trans. Wireless Commun.*, vol. 18, no. 8, pp. 4157–4170, Jun. 2019.
- [13] H. Guo, Y.-C. Liang, J. Chen, and E. G. Larsson, "Weighted sum-rate maximization for reconfigurable intelligent surface aided wireless networks," *IEEE Trans. Wireless Commun.*, vol. 19, no. 5, pp. 3064–3076, May 2020.
- [14] Q. Wu and R. Zhang, "Intelligent reflecting surface enhanced wireless network via joint active and passive beamforming," *IEEE Trans. Wireless Commun.*, vol. 18, no. 11, pp. 5394–5409, Aug. 2019.
- [15] Y. Wang, H. Lu, D. Zhao, Y. Deng, and A. Nallanathan, "Wireless communication in the presence of illegal reconfigurable intelligent surface: Signal leakage and interference attack," *IEEE Wireless Commun.*, vol. 29, no. 3, pp. 131–138, Jun. 2022.
- [16] W. Tang et al., "MIMO transmission through reconfigurable intelligent surface: System design, analysis, and implementation," *IEEE J. Sel. Areas Commun.*, vol. 38, no. 11, pp. 2683–2699, Nov. 2020.
- [17] B. Lyu, D. T. Hoang, S. Gong, D. Niyato, and D. I. Kim, "IRS-based wireless jamming attacks: When jammers can attack without power," *IEEE Wireless Commun. Lett.*, vol. 9, no. 10, pp. 1663–1667, Oct. 2020.
- [18] S. Rivetti, ö. T. Demir, E. Björnson, and M. Skoglund, "Malicious reconfigurable surfaces: How impactful can destructive beamforming be?" *IEEE Wireless Commun. Lett.*, vol. 13, no. 7, pp. 1918–1922, Jul. 2024.
- [19] H. Huang, Y. Zhang, H. Zhang, C. Zhang, and Z. Han, "Illegal intelligent reflecting surface based active channel aging: When jammer can attack without power and CSI," *IEEE Trans. Veh. Technol.*, vol. 72, no. 8, pp. 11018–11022, Aug. 2023.
- [20] H. Huang, Y. Zhang, H. Zhang, Y. Cai, A. L. Swindlehurst, and Z. Han, "Disco intelligent reflecting surfaces: Active channel aging for fully-passive jamming attacks," *IEEE Trans. Wireless Commun.*, vol. 23, no. 1, pp. 806–819, Jan. 2024.
- [21] H. Huang, L. Dai, H. Zhang, C. Zhang, Z. Tian, Y. Cai, A. L. Swindlehurst, and Z. Han, "DISCO might not be funky: Random intelligent reflective surface configurations that attack," *IEEE Wireless Commun.*, vol. 31, no. 5, pp. 76–82, Oct. 2024.
- [22] K. T. Truong and R. Heath Jr., "Effects of channel aging in massive MIMO systems," *J. Commun. Netw.-S. Kor.*, vol. 15, no. 4, pp. 338–351, Aug. 2013.
- [23] G. Li, P. Staat, H. Li, M. Heinrichs, C. Zenger, R. Kronberger, H. Elders-Boll, C. Paar, A. Hu, "RIS-jamming: Breaking key consistency in channel reciprocity-based key generation," *IEEE Trans. Inf. Forensics Secur.*, vol. 19, pp. 5090–5105, Apr. 2024.
- [24] P. Staat, H. Elders-Boll, M. Heinrichs, C. Zenger, and C. Paar, "Mirror, mirror on the wall: Wireless environment reconfiguration attacks based on fast software-controlled surfaces," in *Proc. 2022 ACM on Asia Conf. Comput. Commun. Secur., (ASIA CCS)*, New York, NY, May 2022.
- [25] L. Hu, G. Li, H. Luo, and A. Hu, "On the RIS manipulating attack and its countermeasures in physical-layer key generation," in *Proc. Veh. Technol. Conf., (VTC-Fall)*, Norman, OK, Sep. 2021.
- [26] H. Wang, Z. Han, and A. L. Swindlehurst, "Channel reciprocity attacks using intelligent surfaces with non-diagonal phase shifts," *IEEE Open J. Commun. Soc.*, vol. 5, pp. 1469–1485, Feb. 2024.
- [27] H. Zhang and B. Di, "Intelligent omni-surfaces: Simultaneous refraction and reflection for full-dimensional wireless communications," *IEEE Commun. Surv. Tutor.*, vol. 24, no. 4, pp. 1997–2028 Aug. 2022.
- [28] X. Mu, Y. Liu, L. Guo, J. Lin, and R. Schober, "Simultaneously transmitting and reflecting (STAR) RIS aided wireless communications," *IEEE Trans. Wireless Commun.*, vol. 21, no. 5, pp. 3083–3098, May 2022.

- [29] Y. Li, J. Wang, Y. Zou, W. Xie, Y. Liu, “Weighted sum power maximization for STAR-RIS assisted SWIPT systems,” *IEEE Trans. Wireless Commun.*, early access, Oct. 2024, doi: 10.1109/TWC.2024.3467160.
- [30] Y. Liu, X. Mu, J. Xu, R. Schober, Y. Hao, H. V. Poor, and L. Hanzo, “STAR: Simultaneous transmission and reflection for 360° coverage by intelligent surfaces,” *IEEE Wireless Commun.*, vol. 28, no. 6, pp. 102–109, Dec. 2021.
- [31] Q. Li, M. El-Hajjar, Y. Sun, I. Hemadeh, A. Shojaeifard, Y. Liu, “Achievable rate analysis of the STAR-RIS-aided NOMA uplink in the face of imperfect CSI and hardware impairments,” *IEEE Trans. Commun.*, vol. 71, no. 10, pp. 6100–6114, Oct. 2023.
- [32] S. Zeng, H. Zhang, B. Di, Y. Tan, Z. Han, H. V. Poor, L. Song, “Reconfigurable intelligent surfaces in 6G: Reflective, transmissive, or both?” *IEEE Commun. Lett.*, vol. 25, no. 6, pp. 2063–2067, Feb. 2021.
- [33] H. Zhang, S. Zeng, B. Di, Y. Tan, M. D. Renzo, M. Debbah, Z. Han, H. V. Poor, and L. Song, “Intelligent omni-surfaces for full-dimensional wireless communications: Principles, technology, and implementation,” *IEEE Commun. Mag.*, vol. 60, no. 2, pp. 39–45, Feb. 2022.
- [34] M. F. Imani, D. R. Smith, and P. Hougne, “Perfect absorption in a disordered medium with programmable meta-atom inclusions,” *Adv. Functional Materials*, vol. 30, no. 52, 2005310, Sep. 2020.
- [35] X. Wei, D. Shen, and L. Dai, “Channel estimation for RIS assisted wireless communications: Part I-fundamentals, solutions, and future opportunities,” *Commun. Lett.*, vol. 25, no. 5, pp. 1398–1402, May 2021.
- [36] Q. H. Spencer, A. L. Swindlehurst, and M. Haardt, “Zero-forcing methods for downlink spatial multiplexing in multiuser MIMO channels,” *IEEE Trans. Signal Process.*, vol. 52, no. 2, pp. 461–471, Feb. 2004.
- [37] E. Björnson, M. Bengtsson, and B. Ottersten, “Optimal multiuser transmit beamforming: A difficult problem with a simple solution structure,” *IEEE Signal Process. Mag.*, vol. 31, no. 4, pp. 142–148, Jun. 2014.
- [38] F. Liu, L. Zhou, C. Masouros, A. Li, W. Luo, and A. Petropulu, “Toward dual-functional radar-communication systems: Optimal waveform design,” *IEEE Trans. Signal Process.*, vol. 66, no. 16, pp. 4264–4279, Aug. 2018.
- [39] M. Cui and L. Dai, “Channel estimation for extremely large-scale MIMO: Far-field or near-field?” *IEEE Trans. Commun.*, vol. 70, no. 4, pp. 2663–2677, Apr. 2022.
- [40] D. Tse and P. Viswanath, *Fundamentals of Wireless Communication*. Cambridge Univ. Press, Cambridge, U.K., 2005.
- [41] H. Q. Ngo, E. G. Larsson, and T. L. Marzetta, “Energy and spectral efficiency of very large multiuser MIMO systems,” *IEEE Trans. Commun.*, vol. 61, no. 4, pp. 1436–1449, Apr. 2013.
- [42] A. M. Tulino, S. Verdú, “Random matrix theory and wireless communications,” *Foundations Trends Commun. Inf. Theory*, vol. 1, no. 1, pp. 1–182, Jun. 2004.
- [43] Further Advancements for E-UTRA Physical Layer Aspects (Release 9), document 3GPP TS 36.814, Mar. 2010.
- [44] H. Huang, H. Zhang, Y. Cai, A. L. Swindlehurst, and Z. Han, “An anti-jamming strategy for disco intelligent reflecting surfaces based fully-passive jamming attacks,” in *Proc. IEEE Global Commun. Conf. (GlobeCom’23)*, Kuala Lumpur, Malaysia, Dec. 2023.
- [45] H. Huang, L. Dai, H. Zhang, Z. Tian, Y. Cai, C. Zhang, A. L. Swindlehurst, and Z. Han, “Anti-jamming precoding for disco intelligent reflecting surfaces based fully-passive jamming attacks,” *IEEE Trans. Wireless Commun.*, early access, Feb. 2024, doi: 10.1109/TWC.2024.3360728.